

## MAGNETIC FIELD DIAGNOSIS THROUGH SPECTROPOLARIMETRY \*)

GAUTIER MATHYS

European Southern Observatory, Casilla 19001, Santiago 19, Chile

**ABSTRACT** An original approach, the moment technique, is applied to analyze the shapes of spectral lines of Ap stars recorded in both circular polarizations. The longitudinal magnetic field, the asymmetry of the longitudinal magnetic field, and the quadratic field of the studied stars are derived. From the consideration of these quantities and of their variations through the stellar rotation cycle, constraints on the spatially unresolved structure of the magnetic fields are obtained.

### INTRODUCTION

Spectropolarimetry, and in particular, observation of spectral lines in right and left circular polarizations (RCP and LCP), has for more than 40 years been a privileged tool to diagnose the magnetic fields of Ap (and Bp) stars. However, its use has up to recently been mostly restricted to the determination of a single quantity, the *mean longitudinal magnetic field*, through the measurement of the wavelength shift of spectral lines between RCP and LCP. The diagnostic potential of high-resolution circularly polarized spectra of Ap stars is nevertheless much larger: the *shapes* of the spectral lines contain a wealth of information on the field properties. This information has now become accessible through the availability of low-noise spectra. One approach to its exploitation is described in the present paper: the *moment technique*.

### THE MOMENT TECHNIQUE

In the moment technique, the shapes of the spectral lines observed in the Stokes parameters  $I$  (unpolarized light) and  $V$  (difference between RCP and LCP) are characterized by a set of simple parameters: their moments of various orders about the line centre. The  $n$ th-order moment about wavelength  $\lambda_0$  of a line in Stokes  $I$  (resp.  $V$ ) is denoted  $R_I^{(n)}(\lambda_0)$  (resp.  $R_V^{(n)}(\lambda_0)$ ). Under a number of approximations, the dependences of these moments on atomic parameters pertaining to the corresponding transitions can be interpreted in terms of quantities related to the magnetic field. The theoretical developments

---

\*) Based on observations collected at the European Southern Observatory, La Silla, Chile

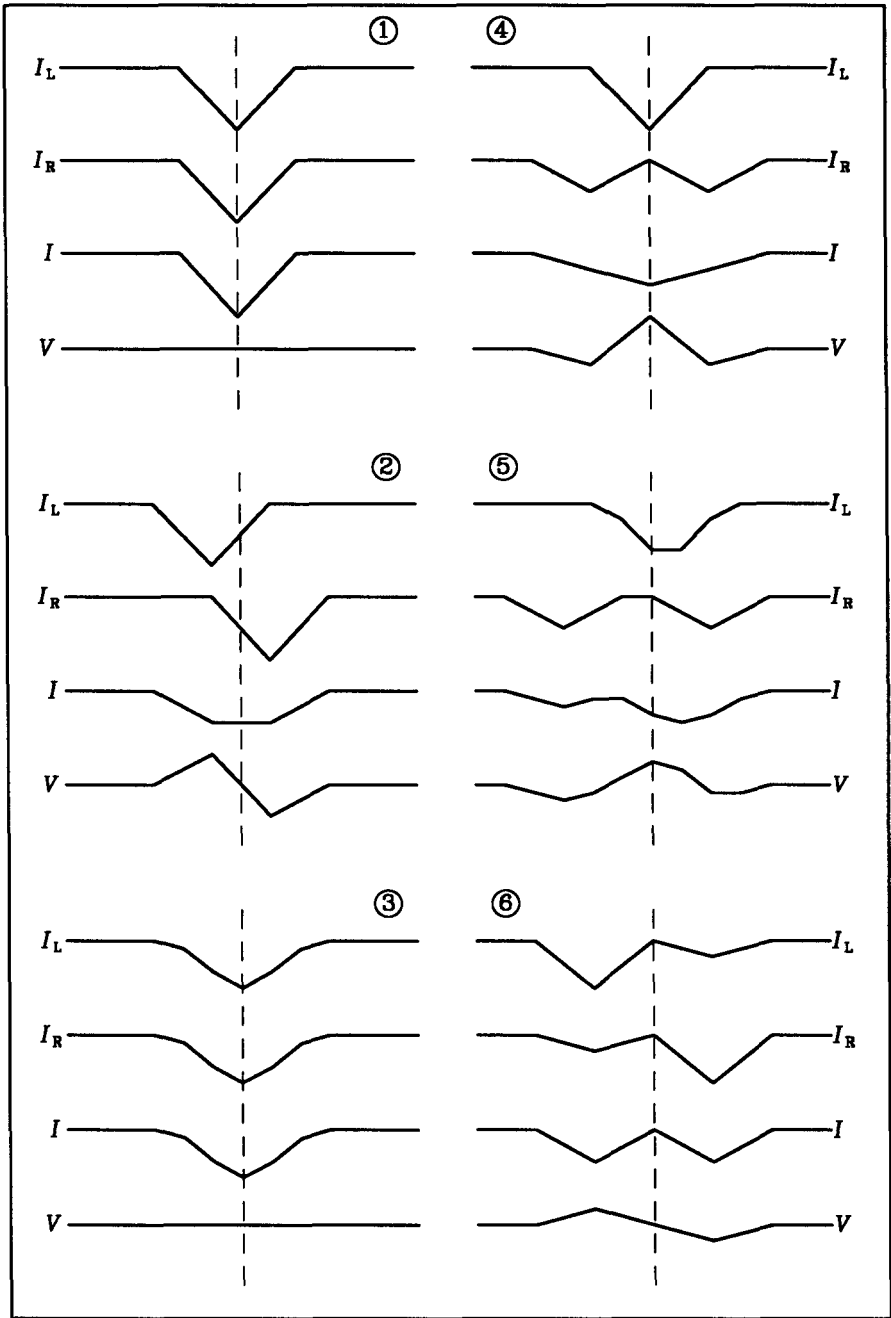


Fig. 1. Simple examples of line profiles in LCP ( $I_L$ ), RCP ( $I_R$ ), Stokes  $I$  and Stokes  $V$  (see text). The dashed vertical line indicates the location of the nominal wavelength of the transition.

TABLE I Moments of the profiles represented in Figure 1

Case	$R_I^{(0)}$	$R_I^{(1)}$	$R_I^{(2)}$	$R_I^{(3)}$	$R_V^{(0)}$	$R_V^{(1)}$	$R_V^{(2)}$	$R_V^{(3)}$
1	$ad$	0	$a^2/6$	0	0	0	0	0
2	$ad$	0	$5a^2/12$	0	0	$a/2$	0	$3a^3/8$
3	$ad$	0	$7a^2/24$	0	0	0	0	0
4	$ad$	0	$2a^2/3$	0	0	0	$a^2/2$	0
5	$ad$	0	$25a^2/24$	$-9a^3/16$	0	$-a/4$	$3a^2/4$	$-3a^3/4$
6	$ad$	0	$7a^2/6$	0	0	$a/2$	0	$3a^3/4$

underlying this interpretation have been presented elsewhere (Mathys 1988, 1989) and will not be repeated here. Instead, an intuitive introduction to the moment technique will be given.

Figure 1 shows six examples of line profiles in LCP, RCP, Stokes  $I$  and Stokes  $V$ , which will hereafter be used to give some intuitive insight into the physical meaning of the notion of moments of the profiles (at least, for the lowest orders). For the sake of simplicity, the unperturbed (i.e., in the absence of a magnetic field)  $I$  profile of the line has been taken triangular. This unperturbed profile is represented in example 1 in the figure. In what follows, its FWHM will be denoted  $a$ , and its depth  $d$ . In the absence of a magnetic field, the  $I$  profile is identical to the RCP and LCP profiles, while  $V$  is uniformly zero.

Examples 2 to 6 in Fig. 1 can be related to some simple magnetic field configurations. If the Zeeman pattern of the line is a triplet, the profiles shown in examples 2 to 5 can, for instance, result from the following configurations. The profiles of case 2 are obtained in a purely longitudinal magnetic field, pointing toward the observer, having an intensity such that the wavelength separation  $\Delta\lambda_\sigma$  between the centres of gravity of the  $\sigma$  components of the line is  $a$ . Case 3 corresponds to a field of similar strength, but purely transversal. Case 4 is obtained when observing two regions having longitudinal fields such that  $\Delta\lambda_\sigma = a$  of opposite polarities, with the region where the field points toward the observer approaching the latter with a velocity corresponding to a Doppler shift  $\Delta\lambda_D = -a$ , while the other region recedes with the same velocity. Case 5 is similar, except that the field pointing away from the observer has a strength such that  $\Delta\lambda_\sigma = 2a$ . Finally, in case 6, the same field configuration as in case 2 is considered, but for an anomalous Zeeman pattern whose  $\sigma$  components look as shown in the figure.

The moments  $R_I^{(n)}(\lambda_0)$  and  $R_V^{(n)}(\lambda_0)$ , for  $n = 0$  to 3, of the line profiles illustrated in Fig. 1 are listed in Table I. The physical meaning of the moments of orders 0 and 1 is rather straightforward. The 0th-order moments are the areas between the continuum and the line profile: for Stokes  $I$ , this is the line equivalent width, which is independent of the magnetic field, while for Stokes  $V$ , this area is always zero, due to the antisymmetry of this parameter.  $R_I^{(1)}(\lambda_0)$  is zero, by definition of the central wavelength of the line.  $R_V^{(1)}(\lambda_0)$  is half of the wavelength shift of the line between RCP and LCP. The interpretation of the other moments is a little less straightforward; their meaning can be

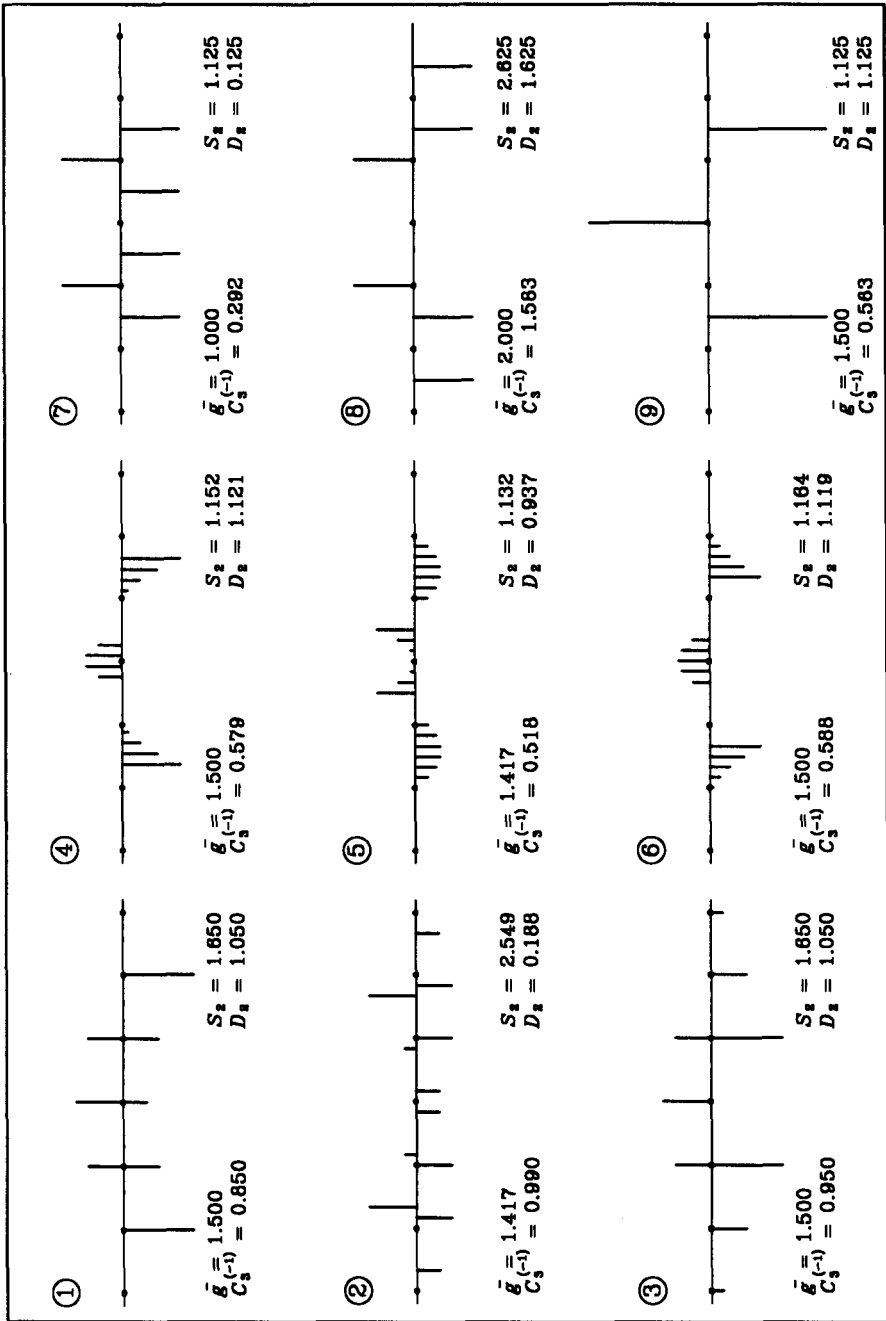


Fig. 2. Some Zeeman patterns, and the global parameters characterizing them. On the wavelength axis, the interval between two consecutive dots is  $H \Delta \lambda_Z$ .

better understood by considering simultaneously the profiles in Fig. 1 and the corresponding values in Table I.  $R_I^{(2)}(\lambda_0)$  characterizes the spread of the intensity distribution in the line about the central wavelength. It is to some extent related to the FWHM of the line, as can be seen from examples 2 and 3: the  $I$  profile has the same zero-intensity width in both cases, but both the FWHM and  $R_I^{(2)}(\lambda_0)$  are larger in the former than in the latter. But  $R_I^{(2)}(\lambda_0)$  is more general than the FWHM; it remains useful in cases when the FWHM becomes meaningless. An illustration of this is provided by the  $I$  profile in example 6: the FWHM cannot be defined, but  $R_I^{(2)}(\lambda_0)$  can, and it is larger than in example 4, because there is more intensity in the profile far from the line centre in case 6 than in case 4.  $R_V^{(2)}(\lambda_0)$  characterizes the difference of width (or more precisely, the difference of spread of the distribution of intensity) between the RCP and LCP profiles. Indeed, it is zero in all examples but 4 and 5, and it is larger in the latter than in the former.  $R_I^{(3)}(\lambda_0)$  gives a quantitative estimate of the asymmetry of the  $I$  profile: its only non-zero value is found for example 5. The meaning of  $R_V^{(3)}(\lambda_0)$  is much less obvious.  $R_V^{(3)}(\lambda_0)$  is to some extent sensitive to the wavelength shift between the centres of gravity of the  $I_R$  and  $I_L$  profiles. This can be seen by computing its value for a configuration similar to that of example 2, but with a different field strength. For instance, if the field is taken to have the same configuration but to be twice as large as in case 2,  $R_V^{(3)}(\lambda_0)$  is multiplied by 4. This contribution has little interest in practice, because it already comes out in  $R_V^{(1)}(\lambda_0)$ . But there is another component to  $R_V^{(3)}(\lambda_0)$ , which can be perceived from the comparison of examples 2 and 6.  $R_V^{(1)}(\lambda_0)$  has the same value in both of them or, in other words, there is the same shift between the centres of gravity of the  $I_R$  and the  $I_L$  profiles in both cases. But  $R_V^{(3)}(\lambda_0)$  is twice as large in case 6 than in case 2. This is clearly due to the difference of the distribution of intensity in the  $I_R$  and  $I_L$  profiles between both cases.

On the other hand, the considered examples show that the moments of the  $I$  and  $V$  line profiles depend on various factors: the intrinsic profile of the line in the absence of a magnetic field, the magnetic field strength and orientation, the Doppler effect undergone by the line forming region (due to stellar rotation), and the Zeeman pattern of the transition. Within the frame of the moment technique, the latter is best characterized by *global* parameters (as opposed to individual shifts and relative strengths of the pattern components). The theoretical developments leading to the introduction of these global parameters have been presented elsewhere (Mathys & Stenflo 1987; Mathys 1989). Here, an intuitive presentation of the physical meaning of those involved in the interpretation of the moments of the profiles up to the third order will be given.

Figure 2 shows Zeeman patterns representative of the various configurations that can be encountered in practice. The values of the corresponding global parameters  $\bar{g}$ ,  $S_2$ ,  $D_2$ , and  $C_3^{(-1)}$  are indicated in the figure. The first of these parameters,  $\bar{g}$ , the effective Landé factor (also called  $z$ -value in older works), has been used for a long time. It is the wavelength shift of the centre of gravity of the  $\sigma_+$  components of the transition with respect to its centre  $\lambda_0$ , in units of  $H \Delta\lambda_Z$ .  $H$  denotes the field strength, and  $\Delta\lambda_Z \equiv k \lambda_0^2$ , with  $k = 4.67 \cdot 10^{-13} \text{ \AA}^{-1} \text{ G}^{-1}$ . The second parameter,  $S_2$ , characterizes the total width of the transition, or more precisely, the spread of all the components, weighted by their strengths. One can indeed see that the triplet of example 9

has (almost) the same effective Landé factor as the anomalous patterns of examples 1 to 6, but that the latter have consistently larger values of  $S_2$ .  $S_2$  is furthermore greater for transition 1 than for transition 4, for 2 than for 5, and for 3 than for 6. On the other hand, the same value of  $S_2$  holds for transition 1 and for transition 3, though the latter is wider, but its outermost  $\sigma$  components are the weakest, while the outermost  $\sigma$  components of transition 1 are the strongest. It is easier to understand the meaning of the difference  $S_2 - D_2$  than that of  $D_2$ .  $S_2 - D_2$  characterizes the spread of the  $\pi$  components, again weighted by their strengths. Indeed,  $S_2 - D_2$  is zero for the triplet 9. It has the same nonzero value for transitions 7 and 8, which have the same  $\pi$  components, but whose  $\sigma$  components have different wavelength shift. It also has a single value for transitions 1 and 3, for which respectively the outermost and the innermost  $\sigma$  components are the strongest. The understanding of  $C_3^{(-1)}$  is a little less straightforward, as it is sensitive to several factors. For given effective Landé factor and mutual separation of the  $\sigma$  components,  $C_3^{(-1)}$  depends on the way in which the strengths of the  $\sigma$  components are ordered (compare patterns 1 and 3). For fixed mutual relation between the  $\sigma$  components, it depends on the shift of their centre of gravity from the line centre (see cases 7 and 8). And as can be seen from the comparison of the pairs of cases of the first two columns of Fig. 2 (1 and 4, etc.),  $C_3^{(-1)}$  depends on the mutual separation of the  $\sigma$  components.

## OBSERVATIONAL RESULTS

The moment technique has been applied to analyze spectra of Ap stars recorded simultaneously in RCP and in LCP with the ESO CASPEC spectrograph fed by the ESO 3.6 m telescope. Up to now, the following quantities related to the magnetic field have been determined: the *mean longitudinal magnetic field*  $\langle H_z \rangle$ , the *mean asymmetry of the longitudinal magnetic field*  $\langle x H_z \rangle$ , and the *mean quadratic magnetic field*  $(\langle H^2 \rangle + \langle H_z^2 \rangle)^{1/2}$ .  $\langle H_z \rangle$  is the average, over the visible stellar hemisphere, of the component of the field vector along the line of sight.  $\langle x H_z \rangle$  is the first-order moment about the plane defined by the line of sight and the stellar rotation axis of the component of the magnetic field along the line of sight ( $x$  is the distance of a point of the stellar disk to the mentioned plane, expressed as a fraction of the stellar radius).  $(\langle H^2 \rangle + \langle H_z^2 \rangle)^{1/2}$  is the square-root of the average over the observed stellar hemisphere of the sum of the square of the modulus of the magnetic field and of the square of its line-of-sight component. All these averages are weighted by the local emergent line intensity.

Physically, the mean longitudinal field is essentially responsible for a wavelength shift of the lines between RCP and LCP. The mean asymmetry of the longitudinal field primarily induces a difference of width of the lines between both circular polarizations. Such differences had already been observed by Babcock (1951), who named the effect the *crossover effect*, but they have not been studied quantitatively up to now. Finally, the quadratic field mostly manifests itself through broadening of unpolarized lines. From the physical interpretation of the moments of the profiles that has been presented above, it can thus be seen that  $\langle H_z \rangle$ ,  $\langle x H_z \rangle$  and  $(\langle H^2 \rangle + \langle H_z^2 \rangle)^{1/2}$  are diagnosed respectively from the first- and second-order moments of the V line profiles,

and from the second-order moments of the  $I$  line profiles. This diagnosis is achieved through application of the following relations:

$$R_V^{(1)}(\lambda_0) = \bar{g} \Delta \lambda_Z \langle H_z \rangle, \quad (1)$$

$$R_V^{(2)}(\lambda_0) = 2 \bar{g} \Delta \lambda_Z \Delta \lambda_R \langle x H_z \rangle, \quad (2)$$

and

$$R_I^{(2)}(\lambda_0) = \Psi^{(2)} + \Delta \lambda_R^2 / 5 + (1/4)(3 S_2 + D_2) \Delta \lambda_Z^2 (\langle H^2 \rangle + \langle H_z^2 \rangle). \quad (3)$$

These relations are only approximate. The assumptions that have been made to derive them are discussed elsewhere (Mathys 1988, 1989, and in preparation). This discussion will not be repeated here.

$\Delta \lambda_R \equiv \bar{\lambda}_0 (v_e/c) \sin i$ , where  $v_e$  is the equatorial velocity of the star and  $i$  the inclination of its rotation axis on the line of sight, and  $\bar{\lambda}_0$  is the average wavelength of the studied spectral region.  $\Psi^{(2)}$  contains all the contributions to the second-order moment of the  $I$  profile but those of the magnetic field and of the rotational Doppler effect. It is dominated by the instrumental broadening, and can be regarded as a constant for all the observations considered here. Accordingly, it was determined by combining observations of various stars, to achieve a better accuracy, and it was subtracted from the observed values of  $R_I^{(2)}(\lambda_0)$  prior to any subsequent analysis. Somewhat similarly,  $\Delta \lambda_R$  is constant through the stellar rotation cycles, so that it could be determined accurately by averaging observations of a given star at various phases. Its contribution to  $R_I^{(2)}(\lambda_0)$  was then subtracted before performing the magnetic field determination for each individual observation.

On the other hand, it is straightforward to extract the projected equatorial velocity  $v_e \sin i$  of the studied star from  $\Delta \lambda_R$ . Not only is this an additional information yielded by the analysis, but furthermore, for stars with good published values of  $v_e \sin i$ , this provides a means of testing the applied technique. Comparison of the values of  $v_e \sin i$  determined in this work with reliable values from the literature show an excellent agreement, which supports the validity of the approach used here.

It should also be noted that the quantity that is directly derived from the study of the second-order moment of the  $V$  profiles is *not* the mean asymmetry of the longitudinal field, but rather its product with the projected equatorial velocity,  $v_e \sin i \langle x H_z \rangle$ , which in what follows is called the *crossover*. The determination of  $\langle x H_z \rangle$  from the latter implies an additional step, namely the division by the value of  $v_e \sin i$ , which needs to be independently determined (e.g., from the consideration of  $R_I^{(2)}(\lambda_0)$ ).

Extensive tables of the measurements of the above-mentioned quantities are to be found elsewhere (Mathys 1991, and in preparation). In this presentation, the main trends emerging for them will be summarized. In addition, plots of the measurements against phase are shown in Figs. 3 and 4 for the stars HD 125248 and HD 175362, to illustrate the following discussion.

Twenty-nine stars have been studied in this work, a large fraction of which were repeatedly observed, at up to 24 phases. Comparison of the derived values of the mean longitudinal magnetic fields with those of the literature for stars previously considered by other authors demonstrate the proper operation of the Zeeman analyzer of CASPEC, which was used for the first time. The accuracy of the  $\langle H_z \rangle$  determinations that is achieved in the best cases is of the order of 80 G. It is limited by the spectral resolution of the observations,

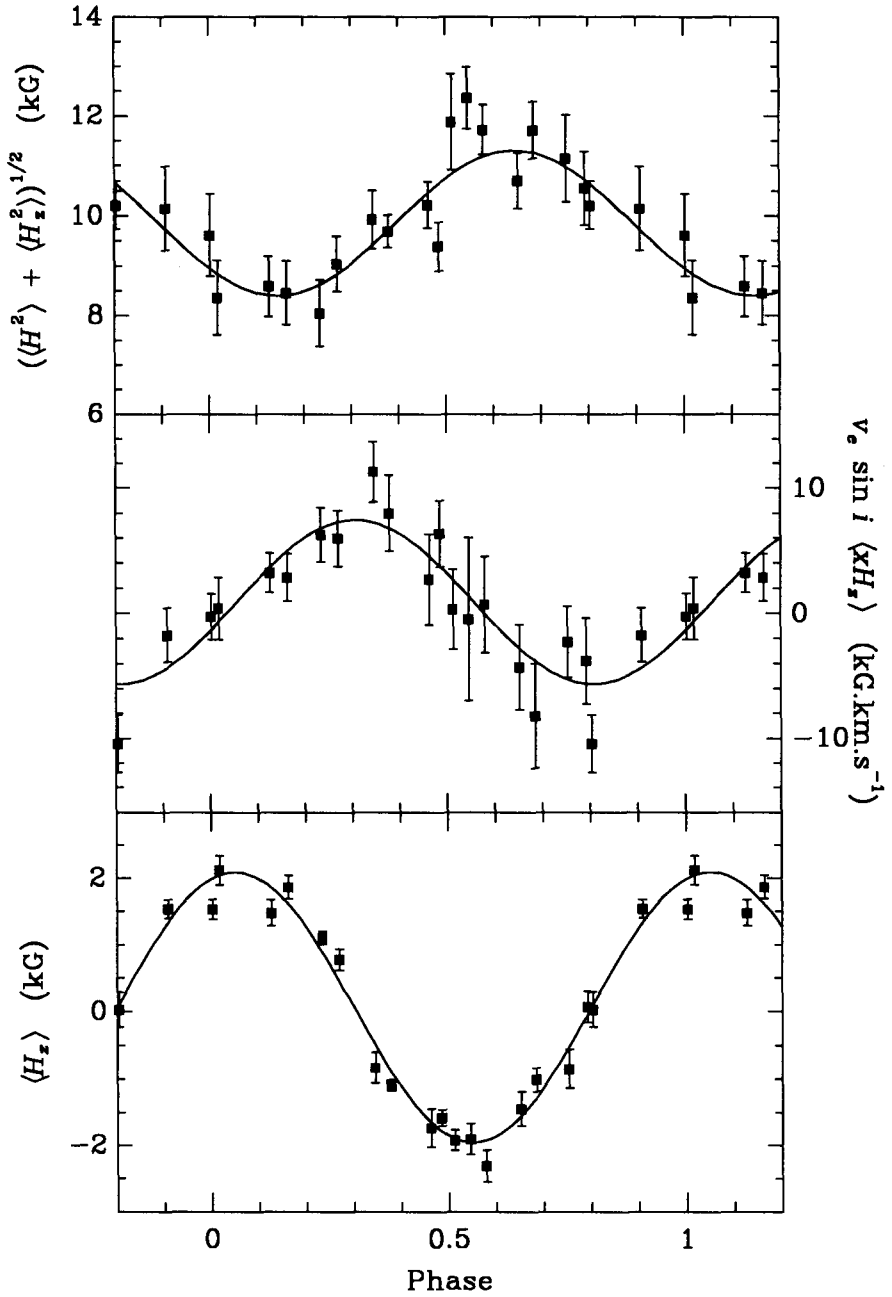


Fig. 3. Observations of  $\langle H_z \rangle$ ,  $v_e \sin i \langle x H_z \rangle$  and  $(\langle H^2 \rangle + \langle H_z^2 \rangle)^{1/2}$  in HD 125248. The curves are least-squares fits of the data by sinusoids.

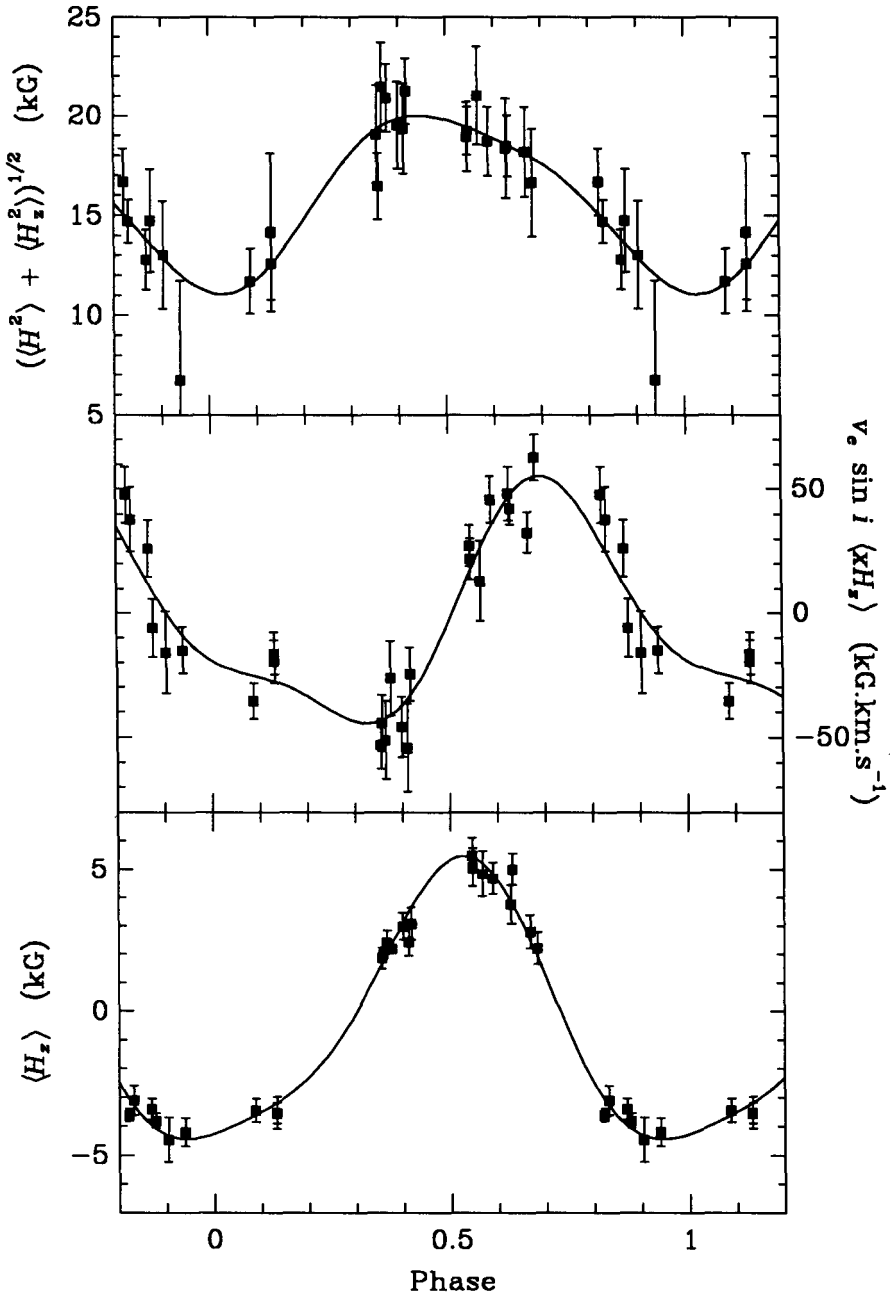


Fig. 4. Observations of  $\langle H_z \rangle$ ,  $v_e \sin i \langle x H_z \rangle$  and  $((H^2) + \langle H_z^2 \rangle)^{1/2}$  in HD 175362. The curves are least-squares fits of the data by superpositions of a sinusoid with the rotation frequency of the star and of its first harmonic.

and consistent with theoretical estimates. Ten of the stars of the sample were observed with (fairly) good phase coverage: HD 83368, HD 96446, HD 119419, HD 122532, HD 125248, HD 137509, HD 137909, HD 147010, HD 153882, and HD 175362. The curves of rotational variation of the longitudinal field of eight of these stars are closely sinusoidal. Figure 3 shows an illustration of this typical behaviour. In the remaining two stars, HD 119419 and HD 175362 (see Fig. 4), the  $\langle H_z \rangle$  variations are definitely nonsinusoidal; rather, they are well represented by the superposition of a sinusoid with the rotation frequency of the star and of a sinusoid with twice that frequency.

Ten only of the twenty-nine stars of the sample have a detectable crossover effect. This is mostly due to the fact that the crossover effect results from the combination of Zeeman and rotational Doppler shifts, so that it can only be observed in stars where the latter is sufficiently large. In particular, stars with periods much in excess of ten days are not expected to show crossover effect. From the consideration of these slowly rotating stars, a lower limit of  $2 \text{ km s}^{-1} \text{ kG}$  to the detectable crossover is derived, which agrees well with the expectations based on an uncertainty analysis taking into account the signal-to-noise ratio and the resolution of the spectra. Eight of the stars where crossover effect was detected were repeatedly observed throughout their rotation cycle. In five of them, the variations of  $\langle x H_z \rangle$  are essentially sinusoidal and symmetric about 0, and they occur in phase quadrature with respect to the variations of  $\langle H_z \rangle$ . Again, the star shown in Fig. 3, HD 125248, is a typical example. Three stars behave differently: HD 137509, HD 147010, and HD 175362 (see Fig. 4). In the latter, the variation of the asymmetry of the longitudinal field, like that of the mean longitudinal field, is better represented by the superposition of a sinusoid with the rotation frequency of the star and of a sinusoid with twice that frequency (no significant crossover effect was detected in the other star whose  $\langle H_z \rangle$  variations are anharmonic, HD 119419). HD 147010 is possibly another case where the variations of  $\langle x H_z \rangle$  are better represented by the superposition of a sinusoid and of its first harmonic, but these variations are not well defined. Finally, HD 137509 has a very large crossover with pronounced variations, which do not appear symmetric about 0 and which occur with a phase difference of 0.125 with respect to the variations of the longitudinal field. The phase coverage of the observations of this star is however rather poor, and the adopted value of its period is somewhat ambiguous (it might be a  $1 \text{ d}^{-1}$  alias of the true value), so that further observations would be needed.

For twenty-three stars of the sample, meaningful values of the quadratic field could be determined. The lower limit of detection of the quadratic fields, set by the spectral resolution and the signal-to-noise of the observations, is of the order of 5 kG. The observed quadratic fields range from this value up to 37 kG, in the star HD 137509. The magnetic field of this star appears to be the second strongest known field in Ap stars. Quadratic field values derived for stars where resolved magnetically split lines are observed in higher-dispersion spectra are consistent with the values of the mean field modulus  $\langle H \rangle$  measured in those stars from the line splitting.  $(\langle H^2 \rangle + \langle H_z^2 \rangle)^{1/2}$  should be somewhat stronger than  $\langle H \rangle$ , due to the fact that it contains contributions from the square of the longitudinal field and from the variance of the field modulus over the stellar disk ( $\langle H^2 \rangle = \langle H \rangle^2 + \sigma^2(H)$ ). This is indeed what is found for the seven stars of the present sample having resolved magnetically split lines. An

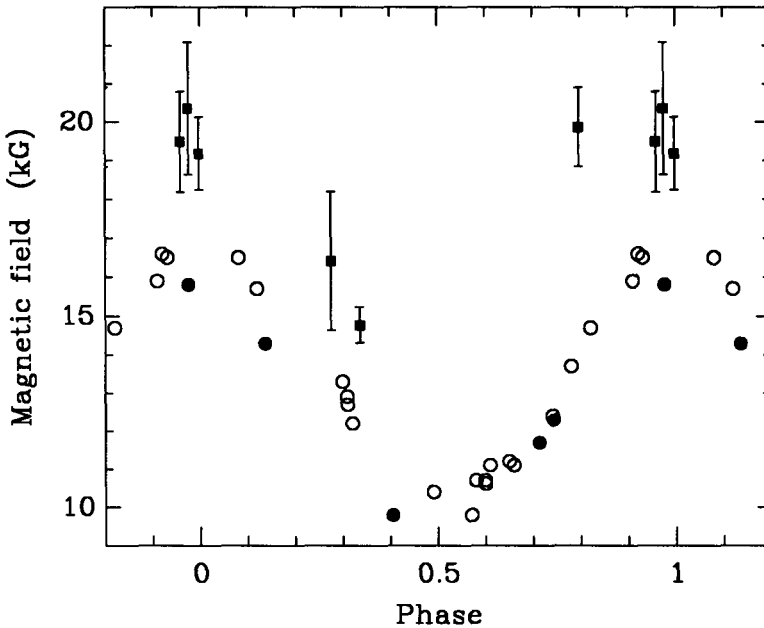


Fig. 5. Observations of the magnetic field of HD 126515. Squares: mean quadratic field  $((H^2) + \langle H_z^2 \rangle)^{1/2}$ . Circles: mean field modulus  $\langle H \rangle$  [open symbols: data from Preston (1970); filled symbols: data from Mathys *et al.* (1992)].

example of this is shown in Fig. 5, in the case of HD 126515.

For nine stars, repeated determinations of  $((H^2) + \langle H_z^2 \rangle)^{1/2}$  were performed throughout the rotation cycle. The variations appear to be satisfactorily represented by a sinusoid with the rotation frequency of the star, or by the superposition of such a sinusoid and of its first harmonic. In several cases, however, the phase coverage of the observations is not quite sufficient to determine unambiguously the shape of the variations of  $((H^2) + \langle H_z^2 \rangle)^{1/2}$ , which generally have a low amplitude; both types of curves mentioned above appear to be almost as suitable. The extrema (or at least one of them) of the quadratic field seem to coincide in phase with (one of) the extrema of the longitudinal field in HD 119419, HD 147010, and HD 153882. But the absence of a phase coincidence between the extrema of  $\langle H_z \rangle$  and of  $((H^2) + \langle H_z^2 \rangle)^{1/2}$  is often observed. This definitely happens in HD 125248, HD 137509 and HD 137909, and possibly also in HD 83368 and HD 175362.

### CONSTRAINTS ON THE FIELD GEOMETRY

No actual modelling of the spatially unresolved structure of the stellar magnetic fields accounting for the new constraints set by the above-described diagnosis of the field properties has up to now been achieved. As a matter of

fact, such a step would still be premature, since the information contents of the line profiles has not been fully extracted yet (higher-order moments can still be analyzed). Nevertheless, a number of interesting properties of the magnetic fields can already be derived from simple considerations.

The simplest model of the geometry of the magnetic field of an Ap star is the *centred dipole*. Within the frame of this model, one can, consistently with the approximations made to derive them, predict analytically how the quantities  $\langle H_z \rangle$ ,  $\langle x H_z \rangle$ , and  $(\langle H^2 \rangle + \langle H_z^2 \rangle)$  should vary along the stellar rotation cycle. Confrontation of these predictions with the observations permits one to test whether the centred dipole is an acceptable model of the field of the studied stars.

If the stellar field was a centred dipole, the following behaviour should be observed.  $\langle H_z \rangle$  and  $\langle x H_z \rangle$  should vary sinusoidally, the latter reversing symmetrically about 0; these variations should occur in phase quadrature. The variations of  $(\langle H^2 \rangle + \langle H_z^2 \rangle)$  should have the form of the superposition of a sinusoid with the rotation frequency of the star, and of a sinusoid with twice that frequency, with the extrema of the fundamental and two of the extrema of the harmonic coinciding in phase with those of  $\langle H_z \rangle$ . Furthermore, the following relations should be obeyed. Be  $\langle H_z \rangle^+$  and  $\langle H_z \rangle^-$  the maximum and the minimum of the longitudinal field over the rotation period, and  $\langle x H_z \rangle^+$  and  $\langle x H_z \rangle^-$  the extrema of the asymmetry of the longitudinal field. ( $\langle H_z \rangle^+$ ,  $\langle H_z \rangle^-$ ,  $v_e \sin i \langle x H_z \rangle^+$  and  $v_e \sin i \langle x H_z \rangle^-$  all are observable quantities.) Then one should have:

$$v_e \sin i \frac{\langle x H_z \rangle^+ - \langle x H_z \rangle^-}{\langle H_z \rangle^+ - \langle H_z \rangle^-} = \frac{15}{32} v_e. \quad (4)$$

From there, one could derive  $v_e$  and, since the rotation period is known, the stellar radius  $R$ . Comparison of the value of  $R$  derived in that way with the typical value for stars of the same spectral type provides an additional test of the validity of the centred dipole model. Another prediction of this model is that the ratio  $\rho$  between the amplitudes of the fundamental and of the harmonic in the variations of  $(\langle H^2 \rangle + \langle H_z^2 \rangle)$  should be equal to  $4(1 + r)/(1 - r)$ , where  $r \equiv \langle H_z \rangle^- / \langle H_z \rangle^+$ . This is again a relation between observable parameters, that can be tested.

In the ten stars observed through their rotation cycle, many inconsistencies between these predictions and the observations are found. In HD 83368, though the variations of the quadratic field are not perfectly determined, the phase lag between the extrema of  $\langle H_z \rangle$  and of  $(\langle H^2 \rangle + \langle H_z^2 \rangle)$  appears to differ from 0, by  $2.5\sigma$ . The upper limit of the crossover derived for HD 96446 yields a value of the stellar radius of  $(0.6 \pm 0.2) R_\odot$ , which is of course much too low for a B2 star. The longitudinal field variations of HD 119419 are definitely anharmonic. The mean value of the crossover for HD 122532 differs from 0 at the  $2.4\sigma$  level. The radius of HD 125248 that is derived  $[(1.27 \pm 0.17) R_\odot]$  is too small for an A1 star. Moreover, a phase lag between  $\langle H_z \rangle$  and  $(\langle H^2 \rangle + \langle H_z^2 \rangle)$  departing from 0 by almost  $4\sigma$  is found (it is clearly seen in Fig. 3), and the centred dipole model predicts the double frequency component in the variations of  $(\langle H^2 \rangle + \langle H_z^2 \rangle)$  to have approximately ten times the amplitude of the fundamental (again in total contradiction with the observed behaviour shown in Fig. 3). In HD 137509,  $\langle x H_z \rangle$  does not reverse symmetrically about 0 (at the  $6\sigma$  level), the phase lag between the variations of  $\langle H_z \rangle$  and of  $\langle x H_z \rangle$  is 0.125, and the quadratic field varies in phase quadrature

with respect to the longitudinal field. As already mentioned, however, more observations should be obtained to improve the phase coverage and to check the validity of the adopted value of the period, before these discrepancies can be definitely regarded as real. For HD 137909, a plausible value of the radius is derived, but there is a definite phase shift between the variations of  $\langle H_z \rangle$  and of  $(\langle H^2 \rangle + \langle H_z^2 \rangle)$ . The existence of a (related) phase shift between the variations of the mean field modulus (determined from the observation of resolved magnetically split lines) and the longitudinal field has, as a matter of fact, been known for a long time (Wolff & Wolff 1970). In HD 147010, there is some evidence that the crossover undergoes a double-wave variation. Even if it eventually proved to vary sinusoidally (if the presumed anharmonicity were only due to the limited number and quality of the available data), the observed crossover would still be much too small to be compatible with the centred dipole model (it would imply that the star has a radius smaller than the solar radius). Furthermore, from the better defined variations of  $(\langle H^2 \rangle + \langle H_z^2 \rangle)$ , the observed  $\rho$ , of the order of 3, is much smaller than the predicted one (10), and the observed phase relation between the fundamental and the harmonic in the variations of  $(\langle H^2 \rangle + \langle H_z^2 \rangle)$  is opposite to what is expected for a centred dipole. In HD 153882, the ratio of  $v_e \sin i$  to  $v_e$  is  $(1.5 \pm 0.2)$ . Finally, the variations of  $\langle H_z \rangle$  and of  $\langle x H_z \rangle$  in HD 175362 are definitely nonsinusoidal.

Thus, the centred dipole model usually does not appear to represent satisfactorily the actual geometry of the magnetic field of the Ap stars. This is not surprising, as this was already known in some cases, in particular for the four stars with resolved magnetically split lines that have been observed throughout their rotation cycle (Landstreet 1980, and references therein). This result is independently confirmed here, for a larger number of stars, which makes it more general.

For a number of stars of the present sample, one can even be more restrictive. Most models of magnetic fields of Ap stars derived up to now belong to one of the two following types. Either the field is assumed to be a dipole offset from the centre of the star along its axis, which goes through the centre of the star. Or it is assumed to be a superposition of collinear low-order multipoles, centred on the centre of the star. The common feature of these two kinds of models is that they both assume that the field has a cylindrical symmetry about an axis going through the centre of the star. For such a symmetric geometry, it can be shown quite generally that the curves of variation of  $\langle H_z \rangle$  and of  $(\langle H^2 \rangle + \langle H_z^2 \rangle)$  should always be symmetric about the phases 0 and 0.5. The latter are defined as the phases when the magnetic axis lies in the plane containing the rotation axis and the line of sight. Observationally these phases should be those of extrema of the longitudinal field and of the quadratic field. The crossover should always be zero, and reverse its sign, at these two phases. The variations of its absolute value should be symmetric about phases 0 and 0.5, too.

Of the ten stars repeatedly observed through their rotation cycle, seven to some extent do not show the above-mentioned symmetries: HD 83368, HD 119419, HD 125248, HD 137509, HD 137909, HD 147010, and HD 175362. Though for one or two of them, additional observations would be welcome to confirm this result, it clearly appears that most of these seven stars have a field that is not cylindrically symmetric about an axis going through the centre of

the star. Thus the "usual" models of magnetic field geometry are not suitable for these stars.

Again, such asymmetries had already been evidenced for the two stars with resolved magnetically split lines HD 126515 (Preston 1970) and HD 137909 (Wolff & Wolff 1970). Their confirmation here for a large fraction of the studied stars indicates that they are rather ubiquitous among magnetic Ap stars.

## CONCLUSIONS

The moment technique is an original method of magnetic field diagnosis from the analysis of the information contents of the shapes of spectral lines recorded in both circular polarizations. Successful applications of this method to the determination of parameters related to the magnetic field have been presented, which have led to the derivation of new constraints on the spatially unresolved structure of the fields. Up to now, only the moments up to order 2 of the  $I$  and  $V$  profiles have been exploited. It should still be possible to extract valuable additional information from the consideration of the third-order moments. This is a rather straightforward extension of the present work, which should be achieved soon. It is much more doubtful that one can make use of the higher-order moments of the profiles with the kind of approach described here, as the intricacy of the interpretation increases very rapidly. A more promising development is the application of the moment technique to the analysis of linearly polarized spectra. The necessary theoretical foundations have already been developed. In practice, the interpretation of the second- and third-order moment of the Stokes  $Q$  and  $U$  line profiles should be quite straightforward. The difficulty may reside in the fact that the polarimetric signal that should be recorded in Stokes  $Q$  and  $U$  is substantially weaker than the one observed in Stokes  $V$ ; lower-noise and higher-resolution may thus be needed to exploit linear polarization information. This will be tested soon, as in the course of the project presented here, a number of linearly polarized spectra have already been obtained for that purpose. It should be stressed that linear polarization studies would strongly enhance the possibilities of constraining the magnetic field geometry, as they would give access to the components of the field in the plane perpendicular to the line of sight (to first order, circular polarization is only sensitive to the component of the field parallel to the line of sight).

Other approaches aiming at diagnosing the magnetic field structure have been recently introduced, which are described in other presentations at this conference. With respect to these methods, which involve time-consuming numerical modelling of line profiles, the moment technique has the originality and the advantage of being simple and fast to use. Therefore, there is no difficulty to apply it to rather large samples of stars repeatedly observed a great number of times. This made possible the achievement of the up to now unrivalled systematic study presented here. From such a kind of study, one can in the future hope to derive a general picture of the magnetism of Ap stars; this would seemingly be much more difficult to achieve using other methods. The counterpart of the relative simplicity of the moment technique may be some loss of accuracy with respect to other approaches. However, this is still to be demonstrated: a comparative application of the moment technique and of

a numerical approach would be very interesting. Moreover, the relative merits of a (possibly) higher accuracy and of the feasibility to study larger samples of stars should be weighed against each other, with regard to the broader scientific context where the magnetic field study belongs. On the other hand, as already noted in other astrophysical contexts (e.g., Castor *et al.* 1981), the use of moments is particularly efficient to characterize the shapes of spectral lines from observational material that has neither a very high signal-to-noise ratio nor a very high resolution. Therefore, the moment technique may be especially well suited, and in particular better suited than numerical line-fitting methods, to the analysis of circular polarization spectra such as those obtained with CASPEC and considered in this work. Still another advantage of the moment technique is that the steps of extraction of information from the line profile and of modelling of the field geometry are uncoupled. This means that the latter of these steps can be repeated as needed, starting from measurements of quantities such as  $\langle H_z \rangle$ ,  $\langle x H_z \rangle$ , or  $(\langle H^2 \rangle + \langle H_z^2 \rangle)^{1/2}$ , which can for instance be readily available in the literature. By contrast, line-fitting methods need to resort to original spectra, which can be somewhat less accessible.

From the point of view of the general knowledge of Ap stars, the main result that emerges from this study is that, in a large fraction of them, the magnetic field does *not* have the property of cylindrical symmetry about an axis going through the centre of the star. This means that one has to go for more complex models of the field than those that have been mostly used up to now. A model like the generalized decentred dipole proposed by Stift (1975) might possibly be suitable. Such models have not up to now been very popular, in particular because they were underdetermined with the available observational data. With new constraints emerging, it is time to turn to them. Obviously, a future continuation of the work reported here, and actually one of its major goals, is to obtain “positive” models of the magnetic fields of the stars of the sample (by contrast with the “negative” models presented here, that is, the exclusion of some models). This is to be the next step in this study, once the third-order moments of the profiles have been analyzed.

## REFERENCES

- Babcock H.W., 1951, ApJ 114, 1  
 Castor J.I., Lutz J.H., Seaton M.J., 1981, MNRAS 194, 547  
 Landstreet J.D., 1980, AJ 85, 611  
 Mathys G., 1988, A&A 189, 179  
 Mathys G., 1989, Fundam. Cosmic Phys. 13, 143  
 Mathys G., 1991, A&AS 89, 121  
 Mathys G., Stenflo J.O., 1987, A&A 171, 368  
 Mathys G., Landstreet J.D., Lanz T., 1992, these proceedings  
 Preston G.W., 1970, ApJ 160, 1059  
 Semel M., 1989, A&A 225, 456  
 Stift M.J., 1975, MNRAS 172, 133  
 Wolff S.C., Wolff R.J., 1970, ApJ 160, 1049